

## ORIGIN OF VARIATIONS IN NICKEL TENOR ALONG THE STRIKE OF THE EDWARDS LODGE NICKEL SULFIDE OREBODY, KAMBALDA, WESTERN AUSTRALIA

CHRISTOPHER HEATH

*Victorian Institute of Earth and Planetary Sciences, Department of Earth Sciences,  
Monash University, Clayton, Victoria 3168, Australia*

YANN LAHAYE<sup>§</sup>

*Victorian Institute of Earth and Planetary Sciences, Department of Earth Sciences,  
Monash University, Clayton, Victoria 3168, Australia*

WILLIAM E. STONE

*St Ives Gold Operations, WMC Resources Ltd., Kambalda, W.A. 6442, Australia*

DAVID D. LAMBERT

*Victorian Institute of Earth and Planetary Sciences, Department of Earth Sciences,  
Monash University, Clayton, Victoria 3168, Australia*

### ABSTRACT

Nickel tenor (Ni concentration in 100% sulfides) varies from 12.5 to 14.5 wt% on the eastern flank, and from 16 to 18 wt% on the western flank of the Edwards lode orebody, Kambalda, Western Australia. The center of the orebody exhibits a large internal variation in tenor, from 9.6 to 18.7 wt% Ni. Tenor variation of this magnitude within a single orebody has not previously been documented at Kambalda. Three models were evaluated for the observed variation. (1) Variation in R factor. This model is supported by a higher nickel tenor within the matrix ores than the massive ores. Pyrolite-mantle-normalized abundances of the platinum-group elements (PGE) are consistent among massive, matrix and disseminated ores. This does not support an R-factor model for tenor variation, because sulfide liquid / silicate melt partition coefficients for the PGE are higher than for Ni ( $D_{\text{PGE}} \gg D_{\text{Ni}}$ ). (2) Variations in oxygen fugacity  $f(\text{O}_2)$ . The  $f(\text{O}_2)$  control on Ni tenor is not supported by geochemical or petrographic observations. The proportion of magnetite is relatively consistent within the orebody, demonstrating no correlation with Ni tenor. (3) Partial redistribution and sulfidation of the nickel ores during upper-greenschist- to lower-amphibolite-facies metamorphism. Evidence includes increased pentlandite abundance correlating with an increase in the abundance of secondary metasomatic pyrite. Some pentlandite grains demonstrate a genetic relationship with carbonate veining, indicating nickel mobility. The large variation in Ni tenor observed within the central domain of the Edwards lode orebody correlates with the ore surface that exhibits the greatest degree of metamorphic heterogeneity. A laser-ablation ICP-MS study of the PGE distribution within sulfides shows that the Ir-group PGE (IPGE) are homogeneously distributed, in contrast to the Pt-group PGE (PPGE). The distribution of Pd reflects the distribution of pentlandite, and the other PGE (Rh, Ru, Pt) and Au seem controlled by PGM and Au-bearing phases. The IPGE show a strong primary magmatic control with distance along the strike of the orebody. Nickel does not demonstrate a correlation with the IPGE, indicating that post-volcanism processes of remobilization partly control the distribution of Ni along strike.

*Keywords:* nickel sulfide, tenor, laser ablation, komatiite, Archean, Otter-Juan ore shoot, Kambalda, Western Australia.

### SOMMAIRE

Les teneurs en nickel (concentration en nickel sur 100% de sulfure) varient de 12.5 à 14.5% (poids) sur le flanc est, et de 16 à 18% sur le flanc ouest du gisement d'Edwards, à Kambalda, en Australie occidentale. Le centre du gisement montre des variations internes importantes des teneurs en nickel, depuis 9.6 jusqu'à 18.7%. De telles variations en teneur n'avaient jamais été

<sup>§</sup> *Current address:* Institut für Mineralogie, Universität Frankfurt, Senckenberganlage 28, D-60054 Frankfurt, Germany.  
*E-mail address:* lahaye@em.uni-frankfurt.de

décrites auparavant à Kamblada. Trois modèles ont été testés pour évaluer les variations en teneur observées. (1) Variation du facteur R. Ce modèle est en accord avec les teneurs plus élevées des minerais en matrice par rapport aux minerais massifs. Les abondances en éléments du groupe du platine, EGP, normalisées par rapport à un manteau pyrolytique, sont semblables dans les minerais massifs, en matrice et disséminés. Ces résultats sont en désaccord avec le modèle du facteur R, étant donné que les coefficients de partage liquide sulfuré / liquide silicaté sont nettement supérieurs pour les EGP que pour le Ni ( $D_{EGP} \gg D_{Ni}$ ). (2) Variation de la fugacité en oxygène ( $f(O_2)$ ). Le contrôle qu'exercerait  $f(O_2)$  sur les teneurs en Ni est en désaccord avec les observations pétrographiques et géochimiques. Les teneurs en magnétite sont constantes au sein du gisement et ne montrent pas de corrélation avec les teneurs en nickel. (3) Une redistribution partielle et sulfuration des minerais de nickel au cours du métamorphisme au faciès schiste-vert supérieur à amphibolite inférieur sont mises en évidence par une augmentation des teneurs en pentlandite de même qu'en pyrite secondaire et métamorphique. Certains grains de pentlandite sont aussi associés à des veines de carbonate, indiquant une mobilité du nickel. Les larges variations observées au centre du gisement d'Edwards sont aussi associées à une grande hétérogénéité métamorphique. Une étude par ablation laser et analyse ICP-MS de la distribution des EGP au sein des minéraux sulfurés montre que les EGP du groupe de l'iridium sont distribués de façon homogène, en contraste avec les EGP du groupe du platine. La distribution du palladium reflète la distribution de la pentlandite, tandis que les autres EGP et l'or semblent régis par la distribution des minéraux du groupe du platine et d'or. La distribution des EGP du groupe de l'Ir fait preuve d'un contrôle magmatique primaire le long de l'axe du gisement. Le nickel ne montre pas de corrélation avec les EGP du groupe de l'iridium, ce qui indique que les processus secondaires de remobilisation post-volcanique contrôlent en partie la distribution du nickel le long de l'axe principal du gisement.

*Mots-clés:* sulfure de nickel, ablation laser, komatiite, Archéen, Otter-Juan, Kambalda, Australie occidentale.

## INTRODUCTION

The Otter-Juan ore shoot is located at the northwestern margin of the Kambalda Dome, approximately 600 km east of Perth in Western Australia's Archean Yilgarn Craton. At Kambalda, high-tenor orebodies are defined as having more than 14 wt% nickel, whereas low-tenor orebodies contain less than 14 wt% nickel (Cowden 1986). Parallel belts of high- and low-nickel tenor orebodies are present on the eastern flank of the Kambalda Dome (Marston & Kay 1980, Woolrich *et al.* 1981). These parallel belts are in fact present intermittently for approximately 15 km, from Victor in the south, through Long, Gibb, Durkin and Otter-Juan. Mineralization is not continuous for the entire 15 km (Fig. 1). The size of the ore shoots within the parallel belts varies from approximately 1.0 million tonnes (Mt) at Victor to 9.9 Mt at Otter-Juan, which is the largest komatiite-associated nickel sulfide (NiS) deposit of its type in the world. Low-tenor ores typically range from 8 to 12 wt% nickel, and high-tenor ores range from 18 to 23 wt% nickel. The Edwards lode represents the down-plunge continuation of the Otter-Juan ore shoot. The Edwards lode is abnormal because its Ni tenor varies more widely, from 9.6 to 18.7 wt%, perpendicular to the strike. Variations in nickel tenor of this magnitude, within a single orebody, have not been previously documented at Kambalda. It is unclear how the Edwards lode fits into the model of parallel belts at Kambalda, and how such internal variations in tenor can be explained by present models on ore genesis. Representative samples have been collected along strike of the orebody and analyzed for their concentrations of major, minor and platinum-group elements (PGE). The distribution of the PGE within sulfides has also been studied *in situ* with the laser-ablation ICP-MS technique. Cor-

relations among Ni tenor, PGE distribution and assemblages of metamorphic minerals will be used to constrain the origin of the variation in Ni tenor within the Edwards lode orebody.

## STRATIGRAPHY

The stratigraphic section of the Kambalda area consists of a basal basaltic unit (the Lunnon Basalt Formation), overlain by a komatiite unit, which locally hosts the NiS mineralization. The komatiite unit is overlain by an upper basaltic unit which, in turn, is overlain by a felsic volcanoclastic and sedimentary unit (Gresham & Loftus-Hills 1981, Swager *et al.* 1995). The Lunnon Basalt Formation is the lowest stratigraphic member at Kambalda. It is comprised of multiple thin (2–30 m) massive and pillowed flows. The formation has been drill-tested to a stratigraphic thickness of 2000 m (Squires *et al.* 1998, Redman & Keays 1985).

The Kambalda Komatiite Formation is divided into two distinct members, the lower nickel-sulfide-bearing Silver Lake Member, and the upper barren Tripod Hill Member. The age of the Kambalda Komatiite Formation is constrained by U-Pb zircon age at  $2709 \pm 4$  Ma (Claoué-Long *et al.* 1988). The Silver Lake Member represents approximately one third of the Kambalda Komatiite Formation and is composed of sequences of one to six magnesium-rich komatiitic lava flow (16–45 wt% MgO, 25–100 m thick). Interflow sulfidic sedimentary sequences are common at the basal contact with the Lunnon Basalt and at flow boundaries within the Silver Lake Member (Gresham & Loftus-Hills 1981, Bavinton 1981). The present assemblage of minerals in the Kambalda Komatiite Formation reflects extensive prograde and retrograde metamorphism at high  $X(CO_2)$ ,  $X(H_2O)$  and fluid:rock ratio.

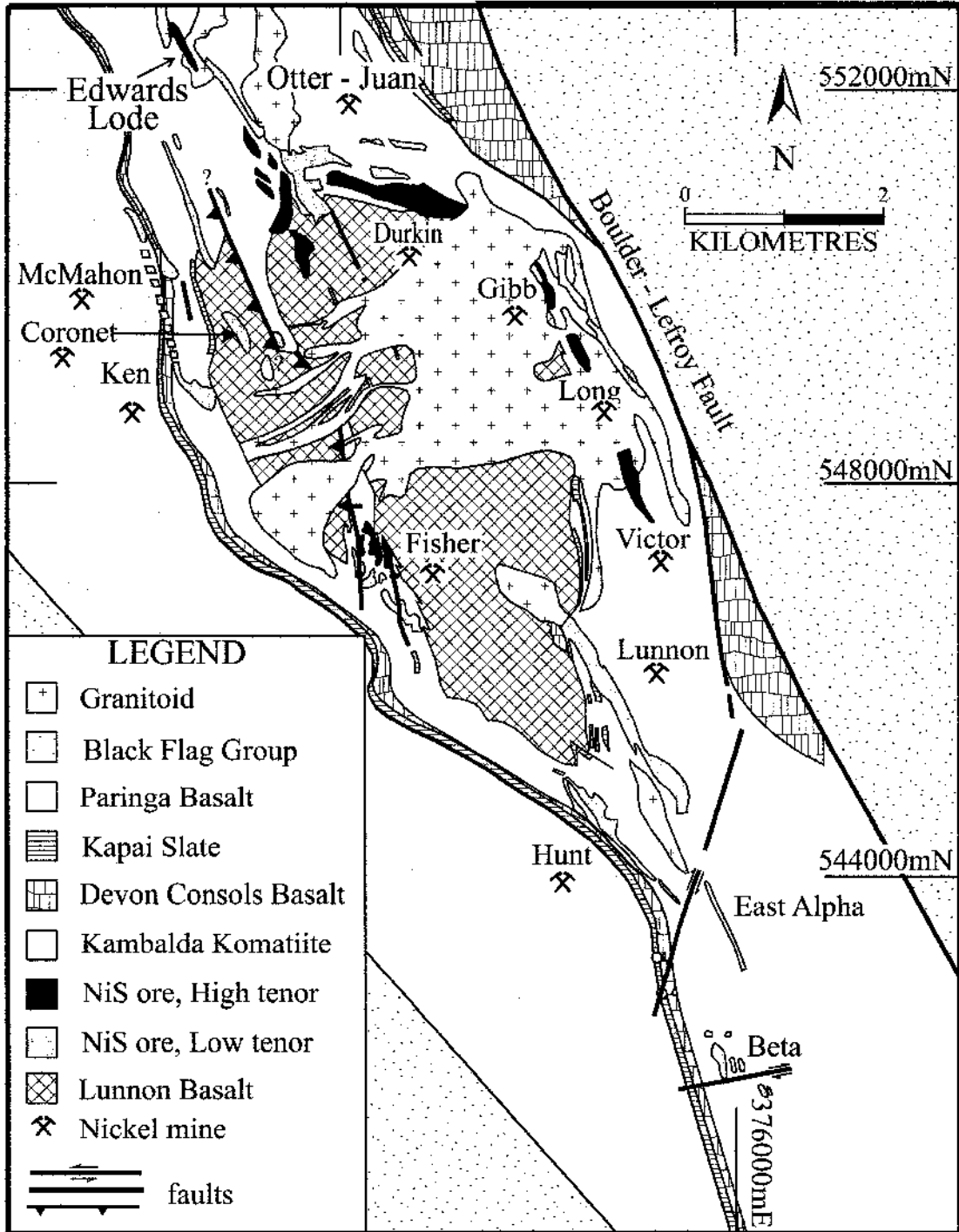


FIG. 1. Geological map of the Kambalda Dome area showing the distribution of rock units and ore shoots as proposed by Marston & Kay (1980). The stratigraphic scheme is from Cowden & Roberts (1995), and the ore-deposit localities are from Stone & Masterman (1998). The Otter-Juan nickel mine is located on the northwestern flank of Kambalda Dome, which is approximately 60 km south of the Eastern Goldfields regional center of Kalgoorlie.

## STRUCTURE AND METAMORPHISM

The Otter–Juan ore shoot is a structurally complex amalgamation of more than 60 individual orebodies. The dip, strike and plunge are highly variable, although the Otter–Juan ore shoot plunges toward the northwest ( $330^\circ$ ) to a depth greater than 1200 m. The projected surface-expression of the Otter–Juan ore shoot is approximately 3 km long, tapering from 1.25 km wide in the southeast to 250 m wide in the northwest. The Edwards lode (62 ore surface) comprises the present northern extent of Otter–Juan ore shoot, and represents the northern end of the Kambalda Dome. The Edwards lode dips from  $20$  to  $25^\circ$  to the southwest and plunges to the northwest. Plunge increases with depth from approximately  $20^\circ$  at the southern extent of the Edwards lode to more than  $45^\circ$  at depth. The Edwards lode has been divided into four ore-surfaces on the basis of hanging-wall and footwall lithology (Fig. 2). The eastern flank, referred to as the M ore surface, consists of massive ore with a basalt footwall and a basalt hanging-wall. Directly west of the M ore surface is the N ore surface, characterized by massive and matrix ore with a basalt footwall and a komatiite hanging-wall. At the western extent of the N ore surface, the basalt footwall rolls away from structurally emplaced ore and forms the W ore surface. This ore surface has a komatiite footwall and a komatiite hanging-wall. The basalt footwall flattens out

at a lower depth than the M and N ore surfaces, forming another concentration of massive ore with a basalt footwall and a basalt hanging-wall. This pinchout ore comprises the western extent of the Edwards lode, and is termed the R ore surface.

Distinct episodes of deformation observed within the Edwards lode can be related to the events of regional deformation around the Kambalda Dome. The first event ( $D_1$ ) produced major north-verging recumbent folds and south- to north-thrust stacking of stratigraphy (Swager *et al.* 1995, Swager 1997, Myers 1992). This event is responsible for the first schistosity ( $S_1$ ) located at the footwall basalt contact in the massive ore within the Edwards lode. The lineations plunge  $37^\circ$  north-northwest in the 31 level of the Edwards lode, indicating elongation of the orebody parallel to its long axis prior to subsequent deformation. The second event ( $D_2$ ) at Kambalda Dome involved east–northeast, west–southwest compression, resulting in the development of west–northwest, east–southeast recumbent folds and thrusts (Cowden & Roberts 1995). Near a sulfide orebody, the  $D_2$  recumbent folding and thrusting produced the ore-confining re-entrant trough structures observed at Kambalda (Archibald 1985, Cowden & Roberts 1990). The basalt pinchouts on the eastern and western flanks of the Edwards lode, confining the M62 and R62 ore surfaces, respectively, are interpreted to be  $D_2$  structures. The deformation is focused on and around

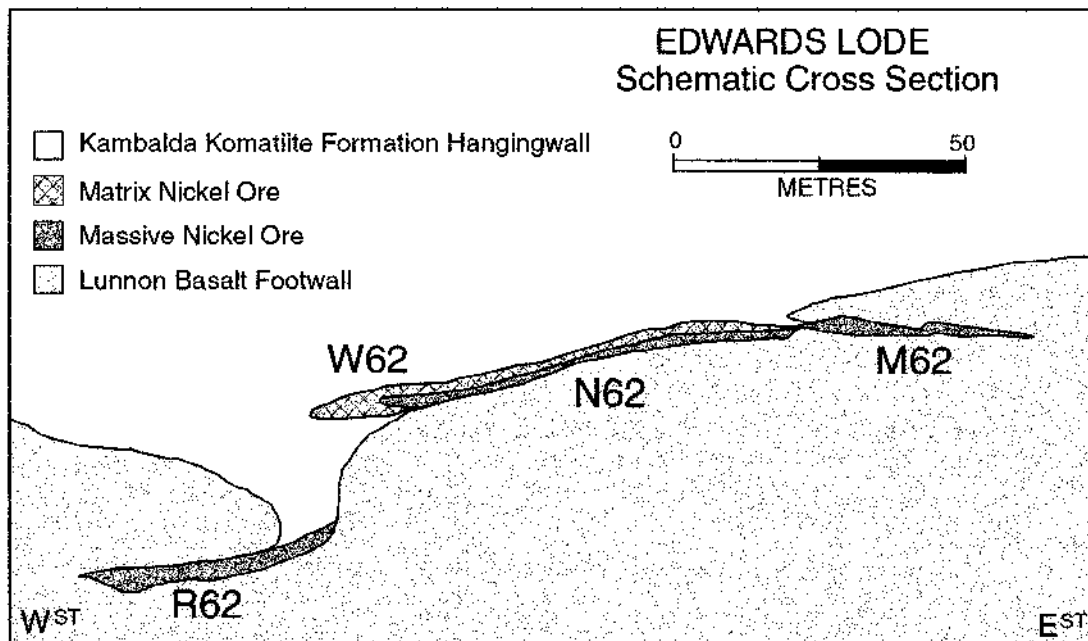


Fig. 2. The Edwards lode, northwest-facing schematic cross-section. Internal ore-surface classifications (M62, N62, W62 and R62) are based on variation in the footwall and hanging-wall lithologies.

the ore horizon, owing to rheological contrast between the massive ore and the Lunnon Basalt. Low-angle thrusts and recumbent folds are activated along these planes of weakness. Massive boudinage structures are present in the M62 ore surface as a result of  $D_2$  recumbent folding. The boudinage structures can be traced down-plunge for at least two mine levels of the Edwards lode. Some of the boudinage structures act as loci for shearing during the third episode of deformation ( $D_3$ ). *En échelon*  $F_3$  folds indicating sinistral movement are regionally associated with large transcurrent faults (Swager *et al.* 1995). The Kambalda Dome is interpreted as a  $D_3$  structure (Archibald 1985).  $D_3$  deformation was identified as a series of upright to steeply northeast-dipping, northwest-trending shears within the M62 and N62 ore surfaces of the Edwards lode. The  $D_3$  shears, which cross-cut  $D_2$  recumbent folding, display limited sinistral strike-slip movement and are commonly associated with local structural remobilization of the ore. The fourth event of deformation ( $D_4$ ) reactivated many of the regional  $D_3$  transcurrent faults, producing locally significant oblique faults that cross-cut and offset the  $D_3$  faults (Swager 1997).  $D_4$  is not considered to play a significant role in the deformation history of the Edwards lode.

The Kambalda Dome underwent upper-greenschist- to lower-amphibolite-facies metamorphism that peaked during  $D_3$  deformation. Peak conditions have been estimated by Bavinton (1979) to be  $520 \pm 20^\circ\text{C}$  and 1 to 4 kbar. Retrograde greenschist-facies metamorphism continued from  $D_3$  to  $D_4$ , along with  $D_3$  hydrothermal alteration and  $\text{CO}_2$  metasomatism (Gresham & Loftus-Hills 1981).

## PETROGRAPHY AND MINERALOGY

The orebodies of the Kambalda Dome are thin, ribbon-like, subparallel linear belts at the base of high-Mg komatiite flows (Cowden & Roberts 1995). At Kambalda, the nickel sulfides reveal vertical zonation in their bulk composition, with a general decrease in sulfide content upward. The massive ore zone, containing more than 80 modal % sulfide (Gresham & Loftus-Hills 1981), is located at the base of the ore profile, in contact with the Lunnon Basalt. The mineralogical assemblage in the massive ore of the Edwards lode is heterogeneous and best discussed in terms of separate ore surfaces within the Edwards lode orebody (Fig. 2).

The M ore surface constitutes the lower-tenor massive ore on the eastern flank of the Edwards lode orebody. Massive ore within the M ore surface pinches and swells, varying in thickness from 2–3 cm to 2–3 m. Pyrrhotite is the dominant sulfide phase ( $46 \pm 7.4$  wt%,  $1\sigma$ , Fig. 3), present as a matrix of small (2–3 mm) grains exhibiting metamorphic  $120^\circ$  triple-point junctions (*i.e.*, a granoblastic texture). Pentlandite occurs as large (2–5 mm) crystals randomly dispersed within the pyrrhotite matrix.

The N ore surface comprises the central domain of the Edwards lode orebody, and is defined as open-contact ore with a basalt footwall and a komatiite hanging-wall. Massive ore within the N ore surface exhibits extremely variable morphology, pinching and swelling from 1–2 cm to 1.5 m. Texturally, the N massive ore is similar to that from the M, with pentlandite ( $41.2 \pm 6.5$  wt%,  $1\sigma$ ) occurring as large grains between 2 and 5 mm in diameter in a pyrrhotite matrix ( $39.3 \pm 9.6$  wt%,  $1\sigma$ ).

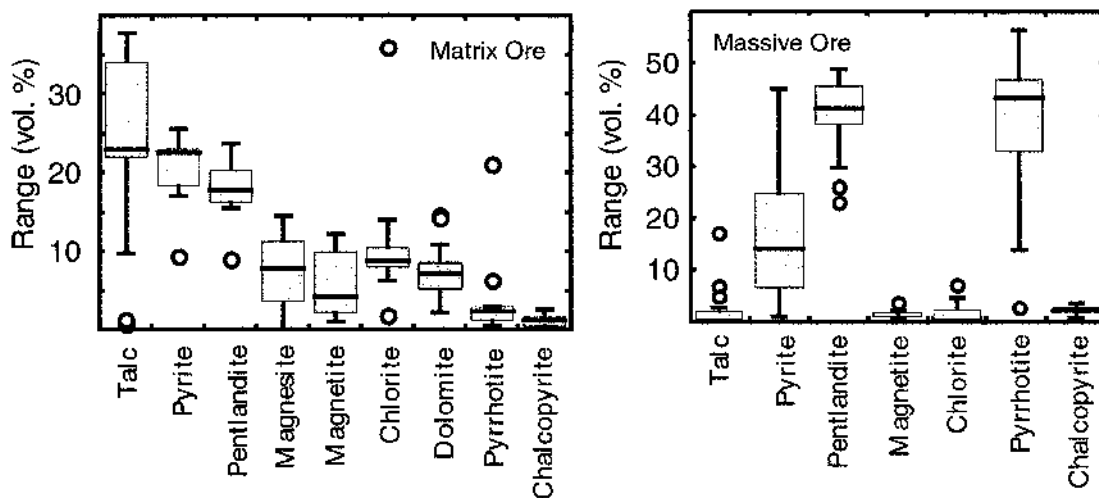


FIG. 3. Ranges and averages for sulfide and silicate abundances, expressed in volume %. The outliers are represented with black circles.

As in the case of the M ore surface, the pyrrhotite matrix is comprised of fine (1–3 mm) grains that exhibit a granoblastic texture. Rare crystals of pentlandite seem to be squeezed within the interstices of recrystallized pyrrhotite at triple-point junctions in a ductile fashion.

The massive ore of the R ore surface comprises the high-tenor western flank of the Edwards lode orebody. The thickness of the massive ore horizon is generally more consistent than in the M and N ore surfaces, varying from a few centimeters to 1.5 m. Sulfide mineralogy is distinct from the M and N ore surfaces, with a higher proportion of pentlandite ( $46.6 \pm 1.6$  wt%,  $1\sigma$ ) and pyrite ( $27.7 \pm 11.3$  wt%,  $1\sigma$ ), and a lower abundance of pyrrhotite ( $22.3 \pm 10.9$  wt%,  $1\sigma$ ). Pyrrhotite occurs as large optically continuous domains, with pentlandite comprising thin (<1 cm) veins.

Pyrite is present as fine-grained metamorphic selvages, at the border of the massive ore, in all ore surfaces within the Edwards lode. Two types of selvages occur. The first consists of randomly dispersed pyrite selvages of roughly equal length and width, varying in size from approximately 5 cm to 18 cm. The second consists of pyrite selvages approximately 5 cm thick, located at the upper and basal contact of the massive ore. The contact-pyrite selvages are commonly continuous for several meters, parallel to the margin of the massive ore. Contacts between pyrrhotite–pentlandite-rich ore and the fine-grained pyrite selvages exhibit sulfide zonation at a microscopic scale. Pentlandite content increases with proximity to the fine-grained metamorphic contact-pyrite selvages, ultimately forming a halo consisting solely of pentlandite surrounding the pyrite selvages. Pentlandite also is present as small lenticular crystals, exhibiting disequilibrium textures with the surrounding pyrite. Pyrrhotite is absent within the pyrite selvages. Euhedral to subhedral porphyroblasts of pyrite, varying from 2 to 6 mm, occur throughout the massive ore horizon associated with pyrite selvages and as discrete crystals.

Carbonate veins within the massive ore are randomly oriented. The crystallization of pyrite and chalcopyrite is commonly located proximal to post-volcanism carbonate veining. A strong correlation is also observed between carbonate veining and small (0.2 mm) pentlandite crystals. However, unusual large crystals of pentlandite (>5 mm) could also be associated with post-volcanism carbonate veining.

Matrix ore (40 – 80% modal sulfide: Gresham & Loftus Hills 1981) generally overlies massive ore and is located in the N62 ore surface of the Edwards lode. The morphological development of the ore is highly variable, with thicknesses varying from 10 cm to over four meters. The thickness of the matrix ore zone broadly demonstrates an inverse correlation with the thickness of the massive ore. In relatively undeformed matrix ore, sulfides occur as fine-grained (0.75 mm) polymineralic aggregates of crystals, with a length-to-width ratio about 1. In high-strain environments, sulfides of the ductile

matrix are stretched and exhibit high aspect-ratios ( $\gg 1$ ). The non-sulfide mineralogy is dominated by an assemblage of talc, carbonate and chlorite replacing primary cumulus olivine. Crystals of relict olivine are commonly replaced by optically continuous talc within the matrix ore. At some localities, the crystals of relict olivine contain very fine-grained lenticular pyrrhotite and pentlandite.

The contacts between massive, matrix and disseminated ore are usually sharp, and locally sheared. At some localities within the Edwards lode, post-extrusion remobilization of sulfides has occurred at the contact between massive ore and the footwall basalt. Chalcopyrite enrichment has always been used as evidence for sulfide remobilization along footwall stringers (Keays *et al.* 1981). A thin band of euhedral grains of chromian spinel, approximately 5–10 mm thick, occasionally occurs at the basal contact of the massive ore within the M ore surface. The chromite band consists of densely packed cumulus grains, with individual crystals approximately 0.1–0.2 mm in diameter. Metamorphic biotite is the dominant non-sulfide mineral associated with the chromite. Chromite is one of the first minerals to crystallize within a sulfide melt and, owing to density contrasts with the sulfide liquid, forms a cumulate layer at the base of the ore horizon (Ewers *et al.* 1976). Magnetite is often concentrated at the massive ore – matrix ore contact within the Edwards lode. Magnetite enrichment occurs at the contact between different ore-zones because of high  $f(\text{O}_2)$  conditions at these localities (Woolrich *et al.* 1981). Variation in rates of oxygen diffusion between sulfide and silicate melts is considered to enhance  $f(\text{O}_2)$  at ore-zone boundaries (Naldrett 1969).

Disseminated ore (<40% modal sulfides) has a similar assemblage of sulfide minerals as the matrix ore. This type of ore is not well exposed within the Edwards lode, as underground development is concentrated along the economically more viable sulfide-rich base of the ore profile. Where present, the disseminated ore horizon varies in thickness between 1 m and >5 m.

Quantitative X-ray diffraction (QXRD) data were used to determine the variation in abundances of the major sulfides along the strike of the Edwards lode. Massive and matrix ore exhibit covariances in sulfide mineralogy along strike. The pentlandite content increases, whereas the pyrrhotite content decreases, corresponding to an increase in metamorphic pyrite (Fig. 4). The observed variation in sulfide abundances results in an increased content of pentlandite within the R ore surface relative to the M and N ore surfaces. Magnetite content is variable within the matrix ore ( $5.5 \pm 3.4$  wt%,  $1\sigma$ ). However, massive ore demonstrates a constant abundance of magnetite along the strike of the orebody.

#### ANALYTICAL TECHNIQUES

Fifty-three samples of ore, each weighing 3–5 kg, were collected perpendicular to the main axis of the

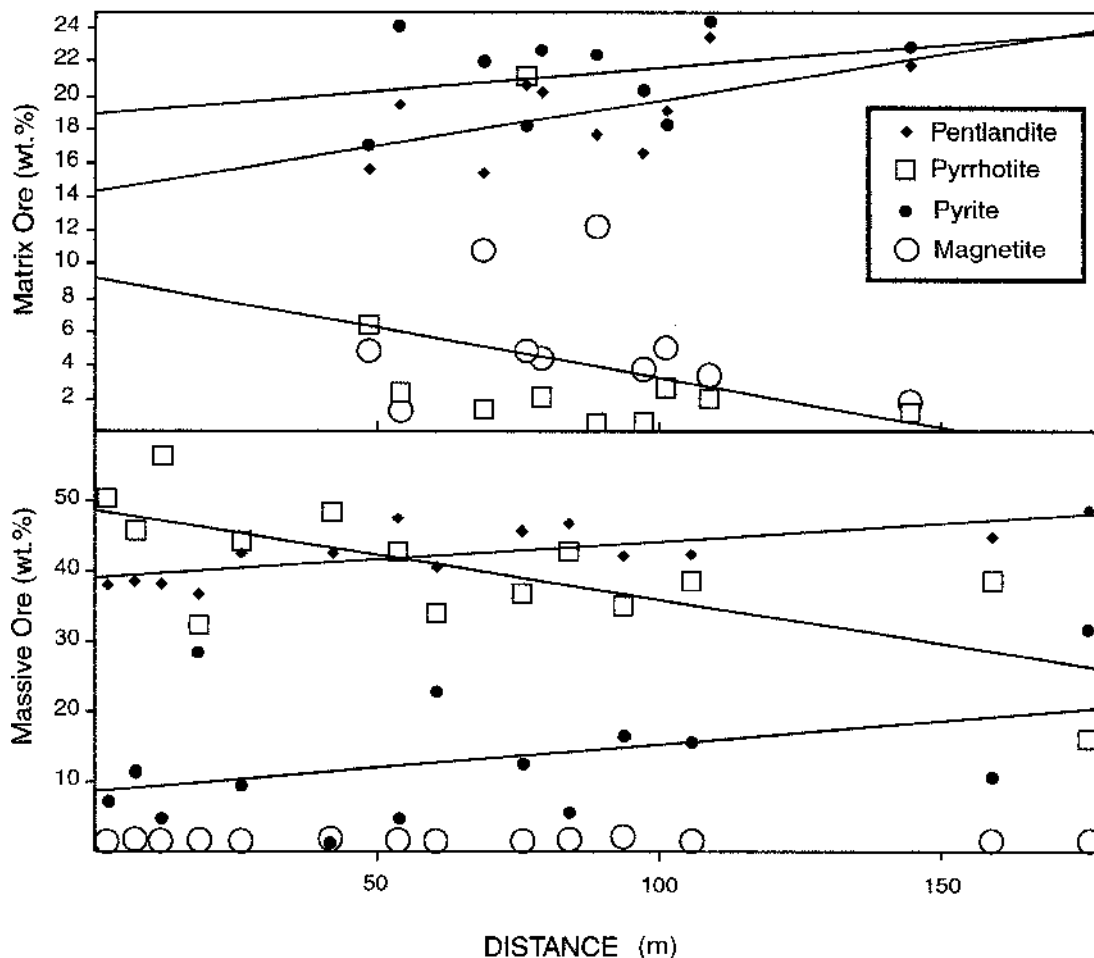


FIG. 4. Along-axis (west-to-east direction) mineralogical variations in pentlandite (black diamond), pyrrhotite (white squares), pyrite (black circles) and magnetite (white circles) within the Edwards lode, as determined from quantitative X-ray-diffraction analysis.

Edwards lode, along a horizontal plane that defined the strike. Sampling orientation was restricted by underground mining operations; however, representative samples of each portion of the deposit at the meter scale were collected. Each sample was analyzed by quantitative X-ray diffraction (QXRD), X-ray fluorescence (XRF), and whole-rock nickel sulfide fire-assay followed by solution analysis using Inductively Coupled Plasma – Mass Spectrometry (ICP–MS) to establish platinum-group element (PGE) concentrations. Duplicate analyses of sulfide whole-rocks provide an estimate of the precision achieved by these analytical techniques. The precision is below 5% RSD for XRF, ICP–MS and QXRD analyses. The PGE contents of individual sulfide phases were determined using High-Resolution – Inductively Coupled Plasma – Mass Spectrometry (HR–

ICP–MS) and laser ablation (LA) in the Department of Earth Sciences, Monash University. The sulfides were ablated *in situ* using polished thick (1 mm) sections. The sulfide phases were analyzed by electron microprobe prior to the laser-ablation analyses. Electron-microprobe analyses were made on a Cameca Camebax SX–50 electron microprobe at the University of Melbourne using wavelength-dispersion spectrometry (20 kV, 19 nA), with data reduced using Cameca PAP corrections. The Fe content of the sulfides determined by electron microprobe has been used as an internal standard for the reduction of the LA–HR–ICP–MS data (Ludden *et al.* 1995). A Cu–Fe–PGE alloy in-house standard has been used as an external standard. Precision (%RSD) on the standard, and limit of detection, are presented in Table 1. The precision is within 15% RSD for the PGE, and 20%

RSD for Au. The limits of detection are between 250 (Rh) and 20 ppb (Ir). The analyses were performed using a Nd-YAG laser, a repetition rate of 4 Hz, an energy at 1 mJ and a crater size of 150  $\mu\text{m}$ . A detailed description of this configuration, optimal instrumental parameters can be found in Lahaye *et al.* (1997). Unlike whole-rock analysis, laser-ablation HR-ICP-MS analysis permits *in situ* quantification and provides some information on the distribution of PGE within individual sulfide phases. Laser-ablation HR-ICP-MS analyses record PGE concentration through time, as the laser progressively ablates a pit into the sulfide grain. Data are recorded as counts per second, which is directly proportional to concentration. Perturbations in the time-integrated signal generated by the spectrometer are interpreted to represent the presence of micrometric platinum-group minerals (PGM). Thus, by this means of analysis we can distinguish PGE present as PGM, and PGE present in solid solution within the host sulfide grain.

The Excel™ tenor-calculation spreadsheet “Tenorcal” of WMC Resources Limited was used to determine the Ni, Cu, and Co tenor values, allowing meaningful comparison of metal content between samples of different sulfide abundance. “Tenorcal” requires XRF whole-rock Ni, Cu, Co, Fe and S values, as well as QXRD-determined pyrrhotite : pyrite ratios. The XRF, QXRD, ICP-MS and Ni-tenor data are presented in Table 2.

### GEOCHEMISTRY

Mine development within the Edwards lode fails to provide ideal along-strike access to the orebody. Samples collected only from the western half of the N62 ore surface place a large down-plunge bias on the dataset. Sample localities, projected to a mean plunge line, thus providing true along-strike representation of geochemical variation, are shown in Figure 5.

The tenor in nickel from the ore within the Edwards lode varies from 9.6 to 18.7 wt%. The average Ni tenor is 15.3 wt%, 14.8 wt% for the massive ores, and 16.4 wt% for the matrix ores. Variation in Ni tenor is observed between and within the M62, N62 and R62 ore surfaces (Fig. 6). The low-tenor eastern flank M62 ore surface varies from 12.5 to 14.5 wt% in Ni tenor, whereas the high-tenor western flank R62 ore surface varies from 16 to 18 wt% in Ni tenor. Massive ore from the open contact N62 ore surface displays a large variation, from 13 to 18 wt% in Ni tenor. Outliers of massive ore with a Ni tenor of 9 to 11 wt% are present at a distance of 75 m from the low-tenor eastern edge of the Edwards lode orebody, within the N62 ore surface. A corresponding outlier of 11 wt% Ni tenor is present within the matrix ore at the same locality (Fig. 6). Mapping at 1:250 scale indicates the presence of a large shear-zone in the south wall of the N62 ore surface at the locality where the outliers were sampled.

TABLE 1. MAJOR ELEMENTS AND PGE CONCENTRATIONS IN SULFIDES, EDWARDS LODE ORE DEPOSIT

	Pyrite	Chalcopyrite	Pentlandite	Pyrrhotite	Std. Prec. LoD
Major-element data by electron-microprobe analysis					
n	4	16	14	20	
S wt%	51.99 ± 0.2	33.72 ± 0.3	32.12 ± 0.8	37.52 ± 0.3	
Fe	44.83 ± 0.8	31.04 ± 0.3	30.53 ± 2.3	60.43 ± 0.3	49.3
Co	3.08 ± 0.8	0.03 ± 0.02	1.66	0.13	-
Ni	0.10 ± 0.26	0.06 ± 0.21	33.9 ± 2.7	0.42 ± 0.18	
Cu	0.03 ± 0.01	31.94 ± 0.5	0.01 ± 0.02	0.01 ± 0.01	50
PGE by laser ablation ICP-MS analysis					
n	4	15	25	26	
Os ppm	63.27	1.82	21.10	21.57	1297 14 0.03
Ir	17.90	0.67	6.99	7.71	973 12 0.04
Ru	28.47	1.16	17.53	13.46	1356 10 0.15
Rh	2.16	17.92	1.25	1.41	1212 5 0.21
Pt	1.39	0.28	1.10	1.21	1214 7 0.07
Pd	0.79	28.70	12.74	9.47	1616 11 0.23
Au	1.15	-	-	-	327 20 0.14

n: number of analyses; -: below limit of detection. Std: standard. Prec.: precision (% RSD). LoD: limit of detection (ppm).

The pyrolyte-mantle-normalized (McDonough & Sun 1995) spectrum for massive and matrix ore is characterized by a depletion in Ni relative to the PGE, as anticipated considering the lower sulfide liquid : silicate melt partition-coefficient of Ni relative to the PGE (Barnes *et al.* 1987). Average pyrolyte-mantle-normalized PGE values for the massive, matrix and disseminated ores are similar (Fig. 7). This lack of variation suggests that similar magmatic processes acted equally within the massive, matrix and disseminated ores. The so-called IPGE (Os, Ir, Ru) demonstrate a strong positive correlation, as anticipated in view of their similar geochemical behavior and immobile nature (Keays & Davison 1976; Fig. 8).

### PGE distribution within sulfide phases

Previous studies of the distribution of PGE within the Kambalda Ni ores have relied on bulk analysis by neutron activation (Keays *et al.* 1981, Cowden *et al.* 1986). On the basis of analyzed separates of sulfide minerals from samples of massive ore from Kambalda, Keays *et al.* (1981) concluded that pentlandite is the dominant host for Pd, pyrite is the dominant host for Ir, and chalcopyrite is an important host for Au. These earlier studies were later criticized by Cowden *et al.* (1986). Based on whole-rock analyses for the PGE, Cowden *et al.* (1986) suggested that Pt, Pd and Au largely occur in discrete mineral phases, in agreement with Hudson & Donaldson (1984). The IPGE are also interpreted to occur in solid solution in pentlandite.

TABLE 2a. WHOLE-ROCK DATA (AS DETERMINED BY XRD AND XRF), EDWARDS LODGE ORE DEPOSIT

Sample	Type	Ni Tenor	Ni XRF	Fe XRF	S XRF	MgO XRF	SiO <sub>2</sub> XRF	Al <sub>2</sub> O <sub>3</sub> XRF	CaO XRF	Pn XRD	Po XRD	Py XRD	Ccp XRD	Mgt XRD	Mgs XRD	Tlc XRD	Chl XRD	Dol XRD
Z67711	Massive	14.30	14.09	46.6	36.9	0.3	0.4	0.1	0.7	41.6	51.0	4.6	2.2	0.7				
Z67712	Massive	13.89	13.36	47.6	36.4	0.3	0.7	0.2	0.6	37.9	50.5	7.4	1.7	2.1				
Z67713	Massive	13.40	13.15	46.8	37.5	0.3	0.5	0.2	0.6	38.1	47.8	10.7	2.3	1.1				
Z67714	Massive	14.77	12.86	40.8	33.0	1.0	3.1	0.6	1.2	36.4	46.0	9.4	1.1	1.4			0.1	
Z67715	Massive	13.09	12.91	45.1	40.0	0.3	0.5	0.1	0.6	36.8	32.7	28.4	1.8					
Z67716	Massive	13.29	13.02	47.4	37.7	0.3	0.5	0.2	0.7	38.7	46.0	11.4	2.3	1.7				
Z67717	Massive	13.45	13.01	45.8	38.8	0.3	0.6	0.4	0.6	37.9	33.7	24.7	2.1	1.2		0.2		
Z67718	Massive	14.05	13.81	45.9	38.1	0.3	0.6	0.1	0.8	40.4	43.4	14.7	1.6					
Z67719	Massive	13.71	13.08	44.8	36.8	0.4	1.0	0.3	0.8	38.3	44.0	13.9	2.3	1.0				
Z67720	Massive	13.75	13.52	48.2	36.6	0.3	0.4	0.2	0.6	39.2	56.3	1.8	1.4	1.1		0.2		
Z67721	Massive	13.59	13.52	48.1	37.6	0.3	0.4	0.2	0.5	38.2	56.5	4.7		0.6				
Z67722	Massive	12.56	12.07	46.2	38.0	0.6	1.4	0.4	0.8	34.9	44.1	17.7	1.4	0.8				
Z67723	Massive	14.82	14.67	45.6	37.6	0.5	0.8	0.2	0.3	42.5	44.5	9.5	3.0	0.6				
Z67724	Massive	16.62	16.55	46.0	36.6	0.4	0.8	0.2	0.3	47.5	46.4	2.6	1.8	1.4		0.3		
Z67725	Massive	15.78	14.51	42.5	34.0	1.3	2.9	0.3	1.8	42.7	48.5	0.7	3.3			0.4		
Z67726	Massive	17.97	16.78	42.1	34.1	2.0	3.3	0.2	0.6	48.8	40.9	2.3	0.7			6.8	0.4	
Z67727	Massive	14.38	13.81	43.4	38.3	1.1	1.6	0.2	1.0	41.3	39.7	14.8	1.4			2.1	0.2	
Z67728	Massive	13.62	13.00	45.7	36.5	1.4	1.5	0.4	1.1	38.1	53.1	7.1				1.0	0.4	
Z67729	Massive	17.35	16.39	42.4	34.9	1.6	2.1	0.5	0.9	47.5	43.2	4.7	1.9			1.3	1.2	
Z67730	Massive	15.36	14.85	44.5	36.4	0.4	0.6	0.1	0.6	42.6	47.9	6.4	2.7			0.4		
Z67731	Massive	14.18	13.91	44.7	38.8	0.6	0.7	0.2	0.6	40.5	34.1	23.0	1.9	0.4		0.2		
Z67732	Massive	9.66	7.78	37.7	35.7	3.2	6.7	1.8	2.0	23.1	13.7	44.9	2.3	1.3		4.7	4.6	
Z67733	Massive	16.57	15.55	42.9	35.7	1.8	2.2	0.3	0.7	45.5	37.1	12.5	1.5	0.7		2.5		
Z67734	Massive	11.37	10.91	46.8	37.9	1.1	1.6	0.4	0.5	29.9	46.8	17.5	2.5	0.9		1.9	0.2	
Z67735	Massive	17.15	15.81	42.8	34.2	1.5	1.6	0.7	1.3	46.7	43.2	5.7	0.5	1.0		0.3	1.8	
Z67736	Massive	14.57	14.24	43.0	39.1	0.9	1.1	0.2	0.5	41.6	26.3	27.5	3.2	0.8		0.4	0.2	
Z67737	Massive	15.39	14.28	43.3	36.1	1.2	1.6	0.5	1.3	41.8	35.1	16.7	0.9	1.7		1.3	2.0	
Z67738	Massive	14.17	12.83	41.3	36.1	2.1	3.7	1.4	0.6	37.7	29.5	24.3	2.6			0.6	3.2	
Z67739	Massive	14.83	14.26	45.5	37.4	0.8	1.7	0.3	0.8	42.4	39.1	15.7	0.2	0.8		0.9	0.2	
Z67740	Massive	17.17	15.28	39.0	34.3	0.7	1.6	0.6	2.0	45.0	38.6	10.8	1.8	1.5		0.3	0.4	
Z67741	Massive	17.16	16.02	44.3	37.7	0.2	0.6	0.1	1.0	46.8	16.7	34.5	1.3					
Z67742	Massive	16.63	15.81	44.9	38.4	0.3	0.4	0.1	0.6	46.1	18.0	34.0	1.6					
Z67743	Massive	18.33	16.71	44.0	36.4	0.5	1.8	0.4	1.0	48.7	18.0	31.5	0.3	1.2				
Z67744	Matrix	14.99	5.37	20.0	15.0	16.1	27.9	1.2	3.6	15.6	6.3	17.0	0.3			37.8	8.5	10.9
Z67745	Matrix	17.30	3.03	18.1	7.2	22.4	25.8	1.8	1.4	8.8	1.1	9.2	0.7	10.0	14.5	34.0	14.0	4.2
Z67746	Matrix	15.48	6.02	25.2	16.7	14.8	25.5	1.2	1.6	17.5	2.3	25.4	0.2	2.0	1.0	36.0	8.7	4.5
Z67747	Matrix	16.07	4.77	22.8	12.5	17.3	18.2	1.2	3.8	13.9	1.9	17.8	0.7	6.8	12.3	26.2	6.2	12.0
Z67748	Matrix	16.12	6.70	26.5	17.4	14.2	16.1	0.9	2.6	19.5	2.5	24.1	1.5	4.0	7.7	22.3	6.7	8.3
Z67749	Matrix	16.49	5.61	22.0	14.4	15.6	24.1	0.9	4.4	16.3		22.8	1.1	1.5		35.5	6.2	14.5
Z67750	Matrix	16.92	1.87	11.6	4.5	24.2	28.1	2.4	4.6	5.4	1.4	5.0	0.4	5.7	9.2	35.0	19.0	14.5
Z67751	Matrix	27.51	0.46	7.0	0.6	28.6	33.4	3.8	3.1	1.3		0.6		5.4	11.4	38.0	29.0	9.7
Z67752	Matrix	15.68	5.30	27.4	14.4	15.2	16.6	1.2	2.3	15.4	1.4	22.0	0.7	9.7	9.0	21.8	9.0	7.1
Z67753	Matrix	11.31	7.11	32.9	25.7	7.9	6.5	0.4	4.4	20.7	21.0	18.2	2.5	5.6	3.6	9.6	1.8	14.2
Z67754	Matrix	16.74	6.92	26.2	17.1	15.6	16.9	1.1	0.7	20.2	2.3	22.7	1.8	4.4	12.2	22.9	8.0	2.0
Z67755	Matrix	17.01	6.10	29.9	15.0	14.1	14.4	1.1	2.1	17.7	0.4	22.4	1.2	12.1	9.2	18.9	8.0	6.9
Z67756	Matrix	17.32	8.91	30.7	21.2	11.2	12.9	0.9	1.4	26.0	2.6	28.0	2.0	3.6	6.2	17.0	7.0	4.4
Z67757	Matrix	17.62	5.72	22.2	13.6	17.4	21.9	1.4	2.6	16.6	0.7	20.2	0.4	3.8	7.3	29.9	10.0	8.3
Z67758	Matrix	17.62	6.58	24.2	15.2	16.8	17.7	1.4	1.9	19.1	2.8	18.3	1.5	5.5	11.2	22.9	10.4	5.9
Z67759	Matrix	17.87	8.08	30.0	18.6	11.2	11.2	7.0	1.7	23.5	2.1	24.6	1.3	3.4	4.1	0.5	35.9	5.3
Z67760	Matrix	18.71	7.49	25.6	16.5	12.8	23.8	1.5	2.4	21.8	1.1	22.9	0.4	1.0	0.0	31.0	11.3	7.8
Z67761	Disseminated		0.27	3.9	0.3	30.5	34.4	1.7	4.3	0.8					23.3	51.0	8.5	13.3
Z67762	Disseminated		0.22	9.4	0.5	8.2	48.0	14.4	8.2	0.7						1.0	7.5	0.3
Z67763	Disseminated		0.09	14.7	0.2	15.1	22.9	17.4	8.1								84.0	

Symbols used: pentlandite Pn, pyrrhotite Po, pyrite Py, chalcopyrite Ccp, magnetite Mgt, magnesite Mgs, talc Tlc, chlorite Chl, dolomite Dol. Proportion of minerals in wt %. Proportions of elements and oxides in weight % Whole-rock data determined by XRF, mineralogical mode determined by quantitative X-ray diffraction.

The analysis of the signal generated by the LA-HR-ICP-MS with time during the ablation provides critical information on the distribution of PGE within the sulfide.

The concentration of Pd in a pentlandite crystal from sample Z67778 demonstrates constant enrichment relative to background levels, indicating that Pd is present in solid solution. Palladium, Rh, Te, Bi, and Sb demon-

TABLE 2b. WHOLE-ROCK DATA (AS DETERMINED BY ICP-MS), EDWARDS LODE ORE DEPOSIT

Sample	Type	Os ppb	Ir ppb	Ru ppb	Rh ppb	Pt ppb	Pd ppb	Au ppb	Cr ppm	Mn ppm	Zn ppm	As ppm	Se ppm	Mo ppm	Ag ppm	Te ppm	Pb ppm
Z67711	Massive	620	410	1600	480	720	1200	85	230	78	21	44.0	34.0	1.2	2.00	8.4	8.0
Z67712	Massive	300	230	800	205	360	1700	40	84	104	22	88.0	41.0	1.6	1.90	10.8	10.0
Z67713	Massive	850	520	2350	1080	2050	2250	125	880	120	38	460.0	34.0	1.9	2.10	9.0	14.0
Z67714	Massive	350	245	860	300	680	1850	70	490	400	58	16.0	54.0	2.5	2.00	18.5	10.0
Z67715	Massive	680	440	1800	470	104	1100	50	265	47	14	14.0	39.0	1.3	2.50	9.6	14.0
Z67716	Massive	500	330	1350	440	2250	1180	55	125	100	23	25.0	39.0	1.6	2.10	11.6	16.0
Z67717	Massive	600	400	1500	330	720	1400	75	120	88	14	102.0	40.0	1.9	2.30	9.8	20.0
Z67718	Massive	780	490	1950	520	1060	1500	35	245	68	15	52.0	34.0	1.3	1.40	9.0	6.0
Z67719	Massive	460	310	1160	390	470	1500	95	980	120	52	30.0	40.0	1.5	2.20	10.6	16.0
Z67720	Massive	350	250	940	330	2350	1850	55	106	116	18	84.0	43.0	2.1	1.60	13.5	14.0
Z67721	Massive	840	540	2350	480	255	960	20	210	68	9	49.0	33.0	1.7	1.00	8.8	12.0
Z67722	Massive	900	560	2400	490	200	1200	35	920	120	32	12.0	33.0	1.6	1.90	10.2	12.0
Z67723	Massive	520	370	1400	440	195	900	110	450	22	41	21.0	35.0	1.5	2.50	6.6	12.0
Z67724	Massive	600	400	1550	460	106	1450	30	185	32	18	11.0	33.0	1.7	1.90	7.4	10.0
Z67725	Massive	440	300	1040	300	165	1500	30	740	185	42	8.0	30.0	2	1.80	11.4	18.0
Z67726	Massive	410	265	1000	450	92	1400	15	250	150	21	9.0	29.5	1.8	1.90	18.0	12.0
Z67727	Massive	255	195	580	265	74	2250	35	150	102	14	11.0	34.0	1.5	1.30	25.5	12.0
Z67728	Massive	600	390	1400	370	135	1850	15	460	210	18	9.0	29.0	1.9	1.40	20.0	12.0
Z67729	Massive	520	340	1250	330	135	1750	20	660	215	32	6.0	27.0	6.4	3.30	22.5	12.0
Z67730	Massive	380	265	960	330	88	880	50	260	74	20	7.0	30.0	1.5	2.30	6.6	14.0
Z67731	Massive	660	410	1600	360	145	1300	90	340	205	24	7.0	29.0	1.5	3.50	6.4	18.0
Z67732	Massive	600	380	1400	320	185	2950	60	2850	430	114	5.0	29.0	4.2	2.80	17.5	14.0
Z67733	Massive	410	290	980	310	94	1350	30	580	155	27	4.0	30.0	2.2	3.00	9.8	12.0
Z67734	Massive	480	330	1140	380	165	1020	35	480	76	21	4.0	32.0	3.1	4.10	8.0	16.0
Z67735	Massive	440	290	1180	350	520	1950	30	400	205	28	4.0	28.5	13.5	2.10	12.0	16.0
Z67736	Massive	640	400	1450	360	215	1650	55	380	62	21	4.0	32.0	1.6	5.20	13.5	16.0
Z67737	Massive	500	340	1180	370	160	1450	25	680	155	25	4.0	30.0	2.7	3.40	13.5	14.0
Z67738	Massive	560	350	1400	370	330	1750	75	980	125	72	5.0	29.0	3	3.80	16.0	18.0
Z67739	Massive	540	360	1450	360	180	1600	25	270	40	12	4.0	35.0	1.7	2.90	17.0	14.0
Z67740	Massive	1200	680	3400	620	350	1400	90	2550	350	92	84.0	36.0	7	2.20	60.0	12.0
Z67741	Massive	900	560	2500	560	680	580	55	70	130	24	130.0	37.0	1.5	1.60	14.0	14.0
Z67742	Massive	1060	640	2950	600	190	300	150	165	37	23	90.0	38.0	1.5	2.10	9.6	16.0
Z67743	Massive	1160	640	4000	2250	3700	3300	12000	940	175	24	1700.0	35.0	3	1.10	10.2	10.0
Z67744	Matrix	230	140	620	145	125	1160	115	450	700	50	6.0	16.0	0.7	1.00	13.5	8.0
Z67745	Matrix	150	100	390	100	72	215	40	840	1180	76	3.0	7.0	0.3	0.70	2.3	6.0
Z67746	Matrix	310	210	740	190	102	390	25	2150	560	84	5.0	16.5	0.8	1.10	7.2	12.0
Z67747	Matrix	58	52	120	72	210	330	35	1650	1250	72	4.0	13.5	0.6	0.90	3.8	10.0
Z67748	Matrix	190	130	460	130	102	320	25	1700	1160	66	2.0	16.0	0.6	1.70	6.4	12.0
Z67749	Matrix	265	170	640	165	64	400	30	1750	1180	82	3.0	13.5	0.5	1.30	2.6	8.0
Z67750	Matrix	44	34	94	36	120	290	15	940	1100	68	2.0	5.0	0.2	0.60	1.1	4.0
Z67751	Matrix	14	10	30	9	20	56		1650	1060	66		1.0		0.20	0.2	
Z67752	Matrix	190	125	450	118	200	460	20	3100	960	80	2.0	14.5	0.5	0.90	4.0	10.0
Z67753	Matrix	295	220	740	275	360	1060	45	3300	1120	62	5.0	22.0	0.9	3.10	6.6	12.0
Z67754	Matrix	235	160	540	150	175	760	50	940	920	78	1.0	16.5	0.7	2.30	3.9	12.0
Z67755	Matrix	140	104	320	120	420	520	25	2850	1200	84		16.5	0.4	1.30	4.7	12.0
Z67756	Matrix	235	150	560	135	160	215	15	3400	920	130	2.0	20.0	1	3.30	6.6	12.0
Z67757	Matrix	320	215	760	210	330	580	45	1250	1000	88		13.0	0.5	1.10	4.5	8.0
Z67758	Matrix	84	70	225	110	165	500	50	960	900	82		17.5	0.9	1.90	7.2	12.0
Z67759	Matrix	265	175	760	220	155	360	20	1800	600	76		16.5	11	2.20	21.5	8.0
Z67760	Matrix	330	205	900	240	400	540	40	370	600	74	28.0	18.5	1.2	0.80	5.2	8.0
Z67761	Disseminated	8	6	10	3	10	8		1000	520	30	2.0		1	0.20	0.3	4.0
Z67762	Disseminated	8	6	22	6	10	10	10	295	1250	94	2.0		0.4	0.40	0.2	6.0
Z67763	Disseminated			4			4		500	1850	130	1.0		0.2	0.10		

strate local covariant concentration, fluctuating with time, within the same grain. This fluctuation is interpreted to indicate the presence of unusual PGM, possible michenerite, PdBiTe, or testibiopalladite Pd(Sb,Bi)Te. A grain of chalcopyrite from the same

sample showed that Rh, Pd and Ag are in solid solution, and that Pd is also associated with Bi, Te and Sb within a PGM, possible sudburyrite (Pd,Pt,Ni)(Sb,Te,Bi). Previous investigators have not documented the presence of discrete *in situ* PGM within the Kambalda ores, but

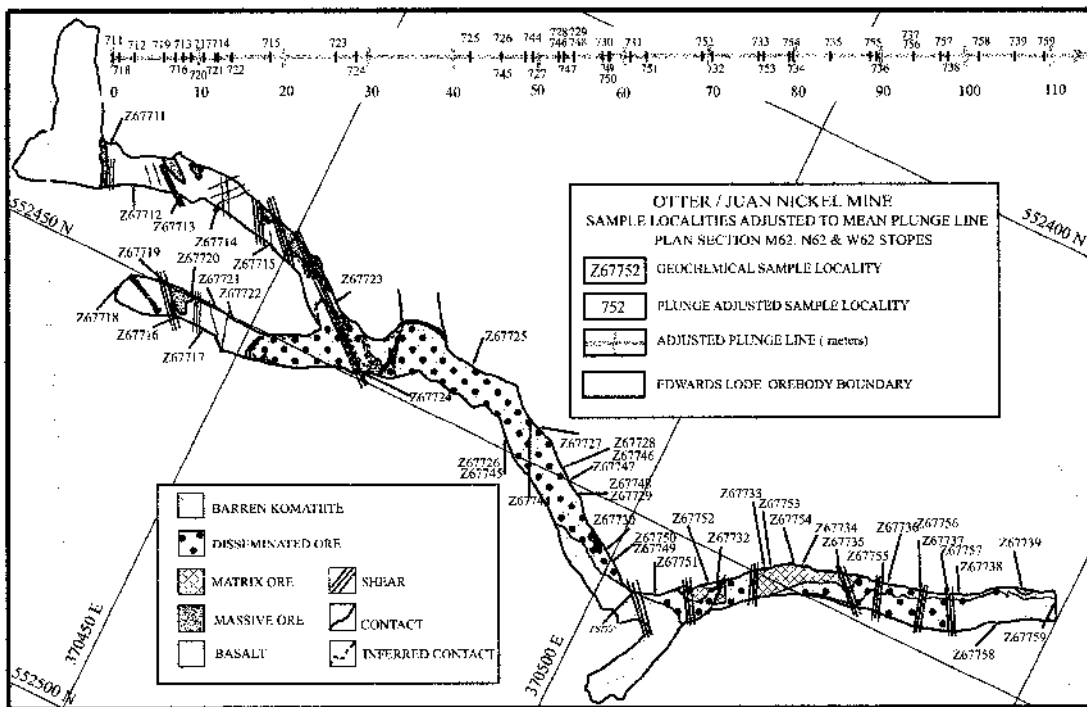


FIG. 5. Plan of the Edwards lode orebody. The geochemical sample localities are adjusted to the plunge-line mean.

rather inferred their existence by analogy with known PGM located within chalcopyrite stringers and telluride-rich quartz-carbonate veins (Hudson 1986).

The pyrolite-normalized (McDonough & Sun 1995) distributions of PGE within (*i.e.*, in solid solution) individual sulfide phases are displayed in Figure 7. The IPGE do not demonstrate the large degree of fractionation among sulfide phases as do the so-called PPGE (*i.e.*, Pt, Pd, Rh). The distribution of Pd reflects the distribution of pentlandite and chalcopyrite, and the Au distribution is controlled by the distribution of pyrite. It should be noted that only a limited number of analyses (four) were conducted on pyrite. On the basis of the modal percentage given by QXRD analysis (Table 2), and the composition of each of the main four sulfide phases present (Table 1), the bulk composition of the massive sulfide ore has been calculated and compared with the average bulk-composition (Table 3). This comparison demonstrates good agreement among the calculated values, based on *in situ* analysis of sulfides for elements such as Os, Ir and Pd. The other PGE (Ru, Rh, Pt and Au) do not seem to be in solid solution in the sulfide, and their recalculated concentrations within the massive sulfide are lower than the average bulk-composition. The analytical data presented here agree with the findings of Ross & Keays (1979), who proposed that

pentlandite is the principal host for Pd, and that Ir is evenly distributed among sulfide phases.

## DISCUSSION

The Edwards lode is abnormal because of its large variation in nickel tenor. The fractional crystallization of monosulfide solid-solution (*Mss*) from a sulfide melt could be responsible for the Ni zonation in the ore environment. Figure 9 represents the variation in Fe, S and Ni (wt%) of the massive, matrix and disseminated ore from the Edwards lode. The ore samples extend along a trend of similar Fe/Ni ratio ( $3.8 \pm 1.8, 1\sigma$ ). However, the massive ore samples are within the *Mss* field. Therefore *Mss* fractionation cannot be responsible for the variation in Ni tenor in Kambalda. Three models were evaluated to explain the observed variation in nickel tenor: (1) variation in R factors, (2) variation in oxygen fugacity, (3) partial Ni redistribution and sulfidation during metamorphism.

### Variations in R factor

The R factor is the mass ratio of silicate melt to sulfide melt, which controls the absolute concentration of chalcophile metals partitioned between the equilibrated

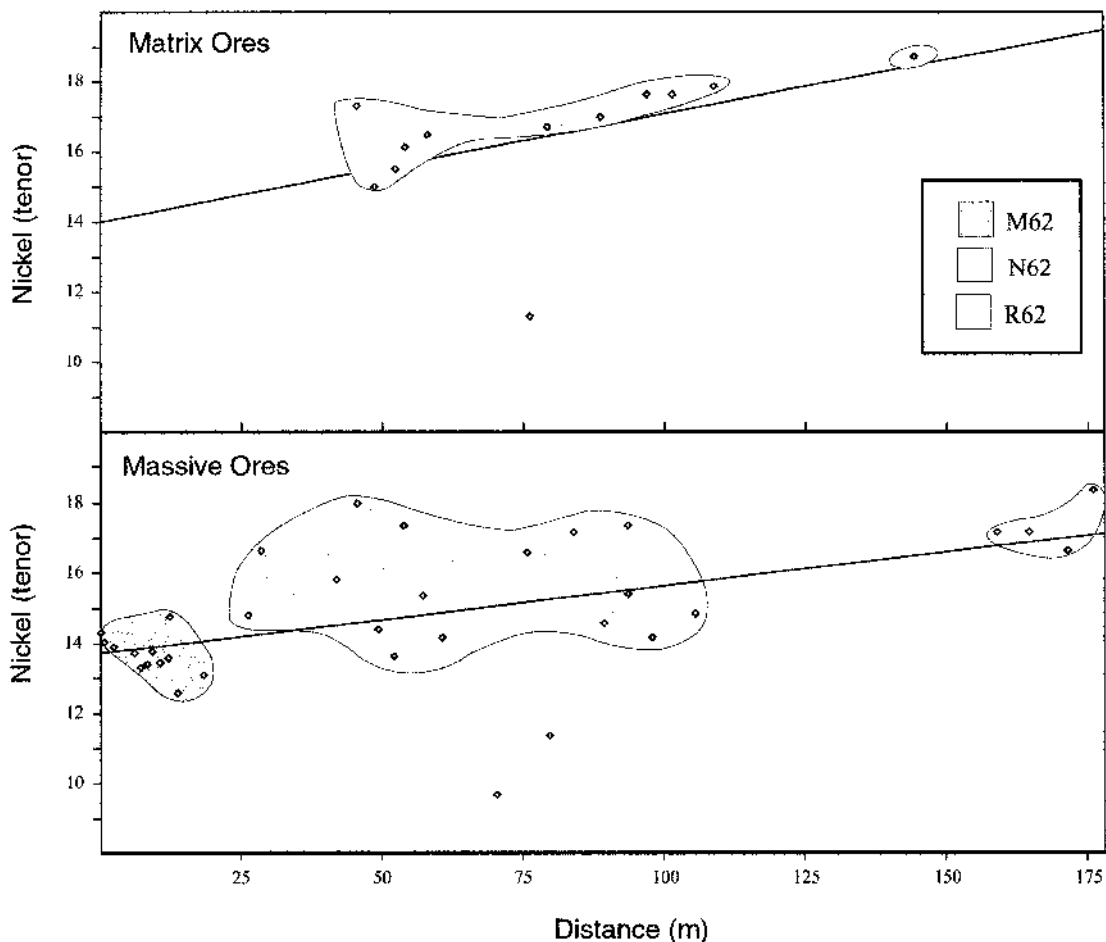


Fig. 6. Along-axis variation in Ni tenor within the Edwards lode. Domains highlight variation in Ni tenor within the M62, N62 and R62 ore surfaces.

melts (Campbell & Naldrett 1979). The higher the R factor, the higher the tenor of Ni in the sulfide melt. The R factor is considered here as a possible mechanism by which variation in Ni tenor may have been produced within the Edwards lode. If the R factor is a major control on variation in Ni tenor, the matrix ore is expected to have a higher tenor of Ni than the massive ore, because matrix sulfides interact with a larger amount of silicate melt (Leshner & Campbell 1993). The different types of ore can therefore be interpreted as having been emplaced successively from a single body of magma, with the lowermost type of ore settling into position first. The ore types would then consist of successive segregation of sulfides from the magmas, and variations in composition would depend on the partitioning of the metals into these successive segregations. The more

chalcophile metals would partition more strongly into the initial segregation, and deplete the melt. Therefore, subsequent segregation of sulfides would be less concentrated. However, the continuous replenishment of komatiitic lavas would have led to the segregation of ore with the same composition. The average tenor of Ni for the matrix ore-zone is calculated at 16.4 wt%, whereas the massive ore is slightly lower, at 14.8 wt%. This disparity in Ni tenor between massive and matrix ore can be explained by the R factor.

The platinum-group elements are much more sensitive to variation in R factor because of their higher partition-coefficients ( $D_{\text{PGE}} \gg D_{\text{Ni}}$ , e.g., Barnes *et al.* 1997). The PGE should therefore exhibit a much greater concentration in the matrix and disseminated ore than in the massive ore. However, the PGE tenors of the

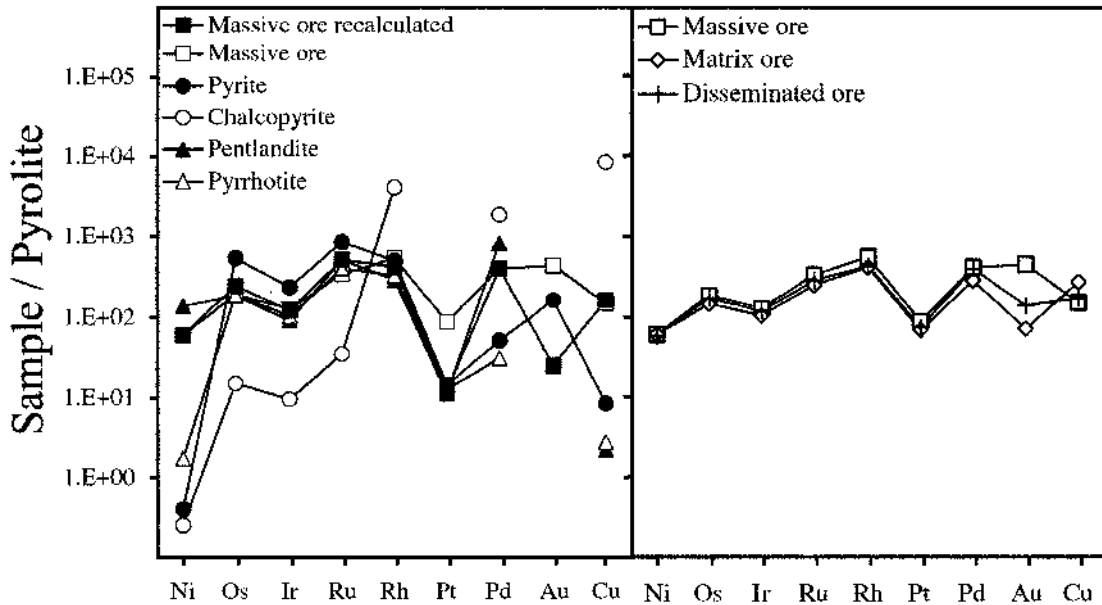


FIG. 7. Pyrolite-normalized (McDonough & Sun 1995) concentrations of the PGE in massive (open squares), matrix (open diamonds) and disseminated ore (crosses). The PGE contents of the sulfides are also shown: pentlandite (black triangles), pyrrhotite (open triangles), pyrite (black circles), chalcopyrite (open circles) and compared with the bulk composition of the massive ore (open squares) and the recalculated concentrations of the massive ore (black squares), based on the concentrations and modal percentage of the sulfide phases.

massive, matrix and disseminated ores are similar if normalized to a pyrolitic mantle source (Fig. 7). A major problem with the R-factor hypothesis is that the tenor within the N62 ore surface is extremely variable (>8%) in a very short distance (<12 m). It is difficult to explain how dynamics of flow of the komatiitic lava could produce such a variation in R factor, and thus in Ni tenor, over such a short distance within a single flow. We conclude that the R factor is unlikely to have controlled the variation in Ni tenor observed within the Edwards lode.

*Variations in oxygen fugacity*

An increase in the oxygen fugacity of a sulfide-saturated silicate melt will increase the tenor of Ni in the immiscible sulfide melt owing to an increase in Fe<sup>3+</sup>:Fe<sup>2+</sup> ratio in the system and the stabilization of Fe<sup>3+</sup> within the silicate melt (Cowden & Woolrich 1987). Cowden (1986) proposed that the variation in Ni tenor within the Kambalda nickel sulfides reflects variations in *f*(O<sub>2</sub>), and that the entire range of ore compositions could be accounted for by variations in *f*(O<sub>2</sub>) of less than one log unit. His interpretation was later criticized by Doyle & Naldrett (1987), who showed that an increase

TABLE 3. AVERAGE COMPOSITION OF THE EDWARDS LODE ORE DEPOSIT

	Massive Ore Average n = 33	Matrix Ore Average n = 17	Disseminated Ore Average n = 3	Massive Ore Recalc.
Major elements by XRF (in 100% S)				
Ni wt%	14.67	14.87	14.34	14.66
Cu	0.55	0.99	0.65	0.61
PGE by fire assay and ICP-MS (in 100% S)				
Os ppm	0.64	0.48	0.57	0.83
Ir	0.41	0.35	0.38	0.38
Ru	1.68	1.22	1.39	2.64
Rh	0.50	0.37	0.38	0.58
Pt	0.61	0.47	0.51	0.89
Pd	1.60	1.09	1.56	1.59
Au	0.44	0.07	0.14	0.03
Average percentage of sulfide phases (in 100% S)				
Cpy vol. %	1.84	2.80	1.84	1.84
Pn	41.90	42.06	46.89	41.90
Py	15.45	46.72	50.61	15.45
Po	40.81	8.41	6.65	40.81

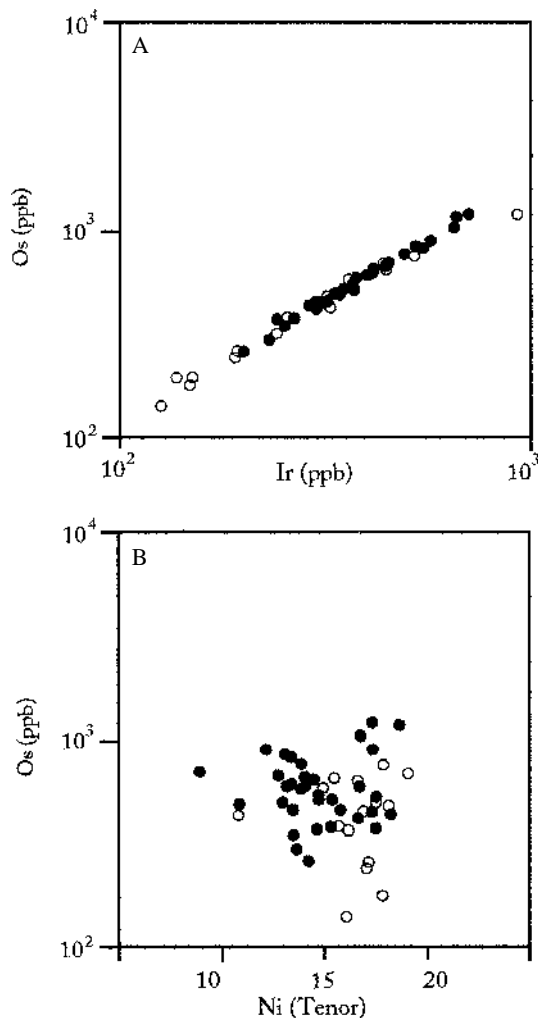


FIG. 8. A. Osmium versus iridium concentrations (ppb). B. Ni tenor (wt%) versus osmium concentration (ppb). Closed symbols represent massive ore, and open symbols represent matrix ore.

in oxygen fugacity will decrease the partition coefficient between the sulfide melt and the olivine. This statement agrees with more recent numerical modeling of the distribution coefficient of Ni between the sulfide and the komatiitic liquid with increasing  $f(\text{O}_2)/f(\text{S}_2)$  (Leshner & Campbell 1993). Variation in  $f(\text{O}_2)$  is evaluated here as a hypothesis for the control of variation in Ni tenor observed within the Edwards lode. Woolrich *et al.* (1981) have observed a correlation between Ni tenor and pyrite abundances among the various orebodies. This correlation was inferred to reflect magmatic oxidation, although metamorphic oxidation cannot be ruled out. An increase in the proportion of pyrite and magnetite would

occur within high-tenor ores with increasing  $f(\text{O}_2):f(\text{S}_2)$ . This change in  $f(\text{O}_2)$  could be related to assimilation of  $\text{H}_2\text{O}$  via unconsolidated sediments during thermal erosion of the flowing komatiitic lava. Petrographic and XRD analysis of the opaque minerals of the Edwards lode indicates that magnetite abundance is consistent along the strike within the Edwards lode massive ore, ranging from 2 to 3 wt% (Fig. 4). Large quantities of magnetite are observed at massive ore – matrix ore contacts, which are interpreted to represent an oxygen sink, a result of differences in rates of oxygen diffusion rates between massive and matrix ores (Naldrett 1969). Such mineralogical evidence for variation in  $f(\text{O}_2)$  as a control of variation in tenor is not present within the Edwards lode. It is also unclear how the flow dynamics of a single komatiitic flow could produce internal variations in  $f(\text{O}_2)$  large enough to yield the observed variation in Ni tenor over such a short distance. We therefore consider it unlikely that variation in  $f(\text{O}_2)$  is responsible for the variation in Ni tenor observed along strike in the Edwards lode.

#### Post-volcanism processes

Post-volcanism processes, such as metasomatism through interaction with sulfur-bearing metamorphic fluids, have been proposed as possible controls on the variation in Ni tenor within the Kambalda Ni sulfide deposits (Keays *et al.* 1981). Many investigators consider post-volcanism processes ineffective at Kambalda Dome because ore shoots of contrasting Ni tenor are present within the same tectonic and metamorphic setting (Leshner & Campbell 1993). Textural and mineralogical observations within the Edwards lode ore zone clearly indicate a large degree of post-volcanism modification of the Ni sulfide assemblages at the deposit scale. Mineralogical evidence for a metamorphic control on Ni tenor includes an increase in abundance of metamorphic pyrite associated with the higher-tenor R62 ore surface, and the presence of metamorphic pentlandite as grains associated with carbonate veining. Note also that the greatest variation in Ni tenor is associated with the N62 ore surface, which exhibits the greatest diversity of metamorphic assemblages and the highest degree of structural deformation. Keays *et al.* (1981) have proposed that the Ni tenor of the matrix ore is on average 7 wt% higher than that in massive ore. This variation was attributed by Keays *et al.* (1981) to a transfer of 5 wt% of the original sulfur from the matrix ore to the massive ore. Variations in Ni tenor of this magnitude, between massive and matrix ore, are not observed within the Edwards lode sulfides. However, the location of fine-grained metamorphic pyrite selvages at massive ore – matrix ore contacts provide evidence for some migration of sulfur.

The IPGE are not greatly affected by post-volcanism processes at whole-rock scale, and inter-IPGE ratios of concentration exhibit consistency along the axis

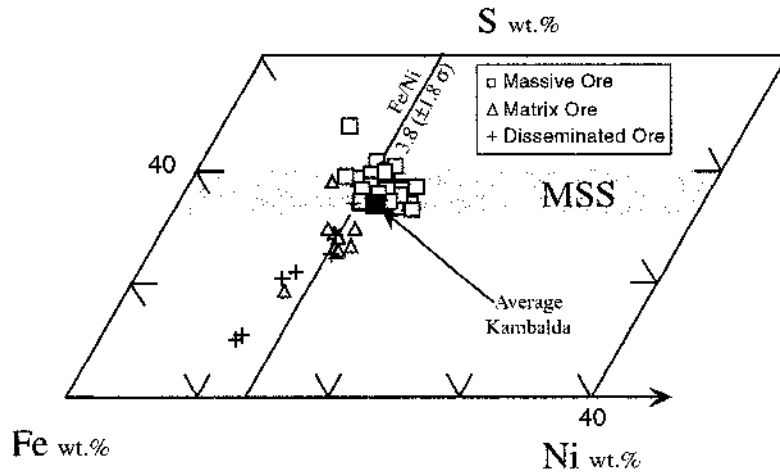


FIG. 9. Variations of the S, Fe and Ni content (wt%) for ore samples from the Edwards lode orebody. The average composition of the Kambalda Dome is also shown (Naldrett 1989). The symbols are as in Figure 7.

of the orebody. This finding suggests a primary magmatic control on the distribution of the IPGE. Nickel tenor and the levels of IPGE (Fig. 8) exhibit no correlation, which implies that different geological processes are responsible for the observed distribution of Ni and the IPGE within the Edwards lode.

Intra-orebody redistribution of Ni during metamorphism is likely to have produced the highly variable Ni tenor observed within the Edwards lode. The solubility of Ni in fluids is affected by temperature, redox condition, salinity, and acidity (Crerar *et al.* 1985). These metamorphic parameters, which are associated with the infiltration of metamorphic fluids within the Kambalda nickel sulfides, are not well understood.

*Comparisons of the Edwards lode with ore shoots of the Kambalda Dome*

The average Ni tenor of the Edwards lode is calculated to be 15.31 wt%, with a standard deviation of 1.99 wt%. Table 4 lists the average Ni tenors for the ore shoots located on the Kambalda Dome, as documented by Leaver (1994), Naldrett (1989), and Leshner & Campbell (1993). Average Ni tenors of ore shoots on the Kambalda Dome were calculated at 14.2 wt% Ni using the data from Naldrett (1989), and 13.9 wt% Ni from the data of Leshner & Campbell (1993). The standard deviation for the two data sets is 2.3 wt% Ni and 1.7 wt% Ni (1σ), respectively. Ross & Keays (1979) proposed that the high Ni tenor of the Durkin shoot (18.2 wt%, Naldrett 1989, Fig. 1) is the result of supergene enrichment processes. The average tenor calculated for the Edwards lode in our study is 15.31 wt% Ni. It falls within the range of the average Ni tenors listed in Table 4.

The high- and low-tenor belt model for Kambalda was originally proposed by Marston & Kay (1980), and later supported by numerous authors (Woolrich *et al.* 1981, Archibald 1985, Gresham 1986, Cowden & Woolrich 1987, Cowden & Roberts 1995, Leshner & Campbell 1993). According to the model, parallel high-Ni (>14 wt%) and low-Ni (<14 wt%) belts are present on the northeastern flank of Kambalda Dome. Statistical analysis of the variation in Ni tenor on Kambalda Dome, and the large intra-ore-shoot variation in Ni tenor highlighted by this study, indicate that the tenor variation is much more complicated than the high- and low-tenor model suggests. The average Ni tenor of an ore shoot at Kambalda is calculated to be 14.05 wt%, with a standard deviation of 2.0 wt% Ni (1σ). This fact ques-

TABLE 4. COMPARISON OF THE Ni TENOR IN THE EDWARDS LODGE WITH THAT IN OTHER ORE SHOOTS OF THE KAMBALDA DOME.

	This study	Leaver (1994)	Naldrett (1989)	Leshner & Campbell (1993)
Edwards lode	15.31			
Lumson			12.8	13.2
Huml		9.8	11.1	11.7
Otter-Juan		11.8	13.8	14.4
Fisher			13.5	14
Long		12.3	14.4	13.8
McMahon			12.2	12
Ken			16.1	15
Durkin			18.2	16.5
Coronet		8.2		
Victor		16.6		
Average	15.3 ± 2	11.7 ± 3.2	14.2 ± 2.3	13.9 ± 1.7

The Ni tenor is expressed in wt%

tions the effectiveness of assigning a high- or low-tenor ranking on the basis of a 14 wt% cut off.

#### CONCLUSION

Nickel tenor varies from 9.6 to 18.7 wt% within the Edwards lode at Kambalda. Geochemical and petrographic evidence indicates that variations in Ni tenor within the Edwards lode is caused by metamorphic, intra-orebody redistribution of Ni. Nickel tenor displays less variation at ore localities in the basalt pinchout on the eastern and western flanks of the Edwards lode. The west-flank R ore surface exhibits internal variation from 16 to 18 wt%. The east-flank M ore surface has a similar variation, but a lower average tenor, between 12.5 and 14.5 wt%. The open-contact N ore surface, located within the center of the Edwards lode, exhibits a large variation in tenor, from 9.6 to 18 wt%. The average Ni tenor for the ore shoots located on Kambalda Dome is calculated to be 14.05 wt% Ni, with a standard deviation of 2.0 wt% Ni ( $1\sigma$ ). Our data suggest that the high- and low-tenor model originally proposed by Marston & Kay (1980) is inappropriate for identifying trends in tenor variation among ore shoots at Kambalda Dome. The arbitrary Ni tenor of 14 wt% used to distinguish the belts equals the average Ni tenor of all Kambalda ore shoots. The average Ni tenor is calculated to be 15.31 wt% for the Edwards lode, which is within one standard deviation of the average Ni tenor for other Kambalda Dome ore shoots. The Edwards lode is therefore considered largely representative of a standard Kambalda-style nickel sulfide deposit.

#### ACKNOWLEDGEMENTS

This study was completed by the first author in partial fulfilment of the requirements for a BSc (Honours) degree in Geology at Monash University. WMC Resources Limited, Kambalda Nickel Operations, provided generous financial support, underground access to the Otter-Juan mine, and authorized the publication of this paper. Critical comments were provided by S. Beresford, E. Curl, S. Fogarty, M. Jane, K. McPhee and B. Palich. Two anonymous reviewers, R.F. Martin and S.-J. Barnes provided constructive reviews that helped to improve the manuscript.

#### REFERENCES

- ARCHIBALD, N.J. (1985): The stratigraphy and tectonic-metamorphic history of the Kambalda Tramways area, Western Australia. *Western Mining Corporation Ltd., unpubl. rep. K/2889*.
- BARNES, S.-J., BOYD, R., KORNELIUSSEN, A., NILSSON, L.P., OFTEN, M., PEDERSEN, R.B. & ROBINS, B. (1987): The use of mantle normalisation and metal ratios. *In Geo-Platinum '87* (H.M. Prichard, P.J. Potts, J.F.W. Bowles & S.J. Cribb, eds.). Elsevier Applied Science, London, U.K. (113-144)
- \_\_\_\_\_, ZIENTEK, M.L. & SEVERSON, M.J. (1997): Ni, Cu, Au, and platinum-group element contents of sulphides associated with intraplate magmatism: a synthesis. *Can. J. Earth Sci.* **34**, 337-351.
- BAVINTON, O.A. (1979): *Interflow Sedimentary Rocks from the Kambalda Ultramafic Sequence: their Geochemistry, Metamorphism and Genesis*. Ph.D. thesis, The Australian National University, Canberra, Australia.
- \_\_\_\_\_. (1981): The nature of sulphidic metasediments at Kambalda and their broad relationships with associated ultramafic rocks and nickel ores. *Econ. Geol.* **76**, 1606-1628.
- CAMPBELL, I.H. & NALDRETT, A.J. (1979): The influence of silicate:sulfide ratios on the geochemistry of magmatic sulfides. *Econ. Geol.* **74**, 1503-1506.
- CLAOUÉ-LONG, J.C., COMPSTON, W., & COWDEN, A.C. (1988): The age of the Kambalda greenstones resolved by ion-microprobe: implications for Archaeological dating methods. *Earth Planet. Sci. Lett.* **89**, 239-254.
- COWDEN, A. (1986): *The Geochemistry, Mineralogy and Petrology of the Kambalda Nickel Sulfide Deposits, Western Australia*. Ph.D. thesis, University of Western Australia, Perth, Australia.
- \_\_\_\_\_, DONALDSON, M.J., NALDRETT, A.J. & CAMPBELL, I.H. (1986): Platinum-group elements and gold in the komatiite-hosted Fe-Ni-Cu sulfide deposits at Kambalda, Western Australia. *Econ. Geol.* **81**, 1226-1235.
- \_\_\_\_\_ & ROBERTS, D.E. (1995): Komatiite hosted nickel sulfide deposits at Kambalda. *In Geology of the Mineral Deposits of Australia and Papua New Guinea* (F.E. Hughes, ed). The Australasian Institute of Mining and Metallurgy, Melbourne, Australia (567-581).
- \_\_\_\_\_ & WOOLRICH, P. (1987): Geochemistry of the Kambalda iron-nickel sulfides: implications for models of sulfide-silicate partitioning. *Can. Mineral.* **25**, 21-36.
- CRERAR, D., WOOD, S., BRANTLEY, S. & BOCARSLY, A. (1985): Chemical controls on solubility of ore-forming minerals in hydrothermal solutions. *Can. Mineral.* **23**, 333-352.
- DOYLE, C.D. & NALDRETT, A.J. (1987): Ideal mixing of divalent cations in mafic magma and its effect on the solution of ferrous oxide. *Geochim. Cosmochim. Acta* **50**, 435-443.
- EWERS, W.E., GRAHAM, J., HUDSON, D.R. & ROLLS, J.M. (1976): Crystallization of chromite from nickel-iron sulfide melts. *Contrib. Mineral. Petrol.* **54**, 61-64.
- GRESHAM, J.J. (1986): Depositional environments of volcanic peridotite-associated nickel sulfide deposits with special reference to the Kambalda Dome. *In Geology and*

- Metallogeny of Copper Deposits (G.H. Friedrich, A.D. Genkin, A.J. Naldrett, J.D. Ridge, R.H. Sillitoe & F.M. Vokes, eds.). Springer-Verlag, Berlin, Germany (63-89).
- \_\_\_\_\_ & LOFTUS-HILLS, G.D. (1981): The geology of the Kambalda nickel field, Western Australia. *Econ. Geol.* **76**, 1373-1416.
- HUDSON, D.R. (1986): Platinum-group minerals from the Kambalda nickel deposits, Western Australia. *Econ. Geol.* **81**, 1218-1225.
- \_\_\_\_\_ & DONALDSON, M.J. (1984): Mineralogy of platinum group elements in the Kambalda nickel deposits, Western Australia. In *Sulfide Deposits in Mafic and Ultramafic Rocks* (D.L. Buchanan & M.J. Jones, eds.). Proc. IGCP Projects 161 and 91, Third Nickel Sulfide Field Conf. (Perth). The Institute of Mining and Metallurgy, London, U.K. (55-61).
- KEAYS, R.R. & DAVISON, R.M. (1976): Palladium, iridium, and gold in the ores and host rocks of nickel sulfide deposits in Western Australia. *Econ. Geol.* **71**, 1214-1228.
- \_\_\_\_\_ , ROSS, J.R. & WOOLRICH, P. (1981): Precious metals in volcanic peridotite-associated nickel sulfide deposits in Western Australia. II. Distribution within the ores and host rocks at Kambalda. *Econ. Geol.* **76**, 1645-1674.
- LAHAYE, Y., LAMBERT, D. & WALTERS, S. (1997): Ultraviolet laser sampling and high-resolution inductively coupled plasma mass spectrometry of NIST and BCR-2G glass reference materials. *Geostandard Newsletters* **21**, 205-214.
- LEAVER, G. (1984): *Mineralisation at the Victor Nickel Mine, Kambalda*. B.Sc. (Honours) thesis, Western Australian School of Mines, Kalgoorlie, Australia.
- LESHER, C.M. & CAMPBELL, I.H. (1993): Geochemical and fluid dynamic modelling of compositional variations in Archean komatiite-hosted nickel sulfide ores in Western Australia. *Econ. Geol.* **88**, 804-816.
- LUDDEN, J.N., FENG, RUI, GAUTHIER, G., STIX, J., SHI, LANG, FRANCIS, D., MACHADO, N. & WU, GUOPING (1995): Applications of LAM-ICP-MS analysis to minerals. *Can. Mineral.* **33**, 419-434.
- MARSTON, R.J. & KAY, B.D. (1980): The distribution, petrology and genesis of nickel ores at the Juan Complex, Kambalda, Western Australia. *Econ. Geol.* **75**, 546-565.
- MCDONOUGH, W.F. & SUN, S.S. (1995): The composition of the Earth. *Chem. Geol.* **120**, 233-253.
- MYERS, J.S. (1992): Tectonic evolution of the Yilgarn Craton, Western Australia. In *The Archean: Terrains, Processes and Metallogeny* (J.E. Glover & S.E. Ho, eds.). Geology Key Centre and University Extension, University of Western Australia, Perth, Australia (265-273).
- NALDRETT, A.J. (1969): A portion of the system Fe-S-O between 900° and 1080°C and its application to sulfide ore magmas. *J. Petrol.* **10**, 171-201.
- \_\_\_\_\_ (1989): *Magmatic Sulfide Deposits*. Clarendon Press, New York, N.Y.
- REDMAN, B. & KEAYS, R.R. (1985): Archean basic volcanism in the Eastern Goldfields Province, Yilgarn Block, Western Australia. *Precamb. Res.* **30**, 113-152.
- ROSS, J.R. & KEAYS, R. (1979): Precious metals in volcanic-type nickel sulfide deposits in Western Australia. I. Relationship with the composition of the ores and their host rocks. *Can. Mineral.* **17**, 417-435.
- SQUIRES, R.J., CAS, R.A.F., CLOUT, J.M.F. & BEHETS, R. (1998): Volcanology of the Archean Lunnon Basalt and its relevance to nickel sulfide-bearing trough structures at Kambalda, Western Australia. *Aust. J. Earth Sci.* **45**, 695-716.
- STONE, W.E. & MASTERMAN, E.E. (1998): Kambalda nickel deposits. In *Geology of Australian and Papua New Guinean Mineral Deposits* (D.A. Berkman & D.H. Mackenzie, eds.). The Australasian Institute of Mining and Metallurgy, Melbourne, Australia (347-356).
- SWAGER, C.P. (1997): Tectono-stratigraphy of the Late Archean Greenstone Terranes in the southern Eastern Goldfields, Western Australia. *Precamb. Res.* **83**, 11-42.
- \_\_\_\_\_ , GRIFFIN, T.J., WITT, W.K., WYCHE, S., AHAMAT, A.L., HUNTER, W.M. & MCGOLDRICK, P.J. (1995): Geology of the Archean Kalgoorlie Terrane – an explanatory note. *Geol. Surv. Western Australia, Rep.* **48**.
- WOOLRICH, P., COWDEN, A. & GIORGETTA, N.E. (1981): The chemical and mineralogical variations in the nickel mineralisation associated with the Kambalda Dome, Western Australia. *Econ. Geol.* **76**, 1629-1644.

Received September 24, 1999, revised manuscript accepted May 3, 2001.